STANEVANSITE, Mg(C$_2$H$_3$O$_3$)$_2$·2H$_2$O, A NEW HYDROUS GLYCOLATE MINERAL, FROM THE SANTA CATALINA MOUNTAINS, TUCSON, ARIZONA, USA

Hexiong YANG[§]

Department of Geosciences, University of Arizona, 1040 E. 4th Street, Tucson, Arizona 85721-0077, USA

Xiangping GU

School of Geosciences and Info-Physics, Central South University, #932, South Lushan Road, Changsha, Hunan 410083, China

Warren LAZAR, Ronald B. GIBBS, and Robert T. DOWNS

Department of Geosciences, University of Arizona, 1040 E. 4th Street, Tucson, Arizona 85721-0077, USA

ABSTRACT

A new organic mineral species, stanevansite, ideally Mg(C$_2$H$_3$O$_3$)$_2$·2H$_2$O, was discovered from the western end of Pusch Ridge in the Santa Catalina Mountains (32° 21′ 42″ N, 110° 57′ 30″ W, at the elevation of 975 m), north of Tucson, Arizona, USA. It occurs as sprays of bladed crystals (up to 0.40 × 0.07 × 0.03 mm). Associated minerals include lazaraskeite, chrysocolla, malachite, wulfenite, mimetite, phosphohedyphane, cerussite, hematite, calcite, microcline, phlogopite, and quartz. Stanevansite crystals are colorless in transmitted light, transparent with white streak and vitreous luster. They are brittle and have a Mohs hardness of ~1½; cleavage is perfect on {100}. Twinning is common on (100). The measured and calculated densities are 1.69(5) and 1.682 g/cm^3, respectively. Optically, stanevansite is biaxial (+), with α = 1.539(5), β = 1.545(5), γ = 1.558(5), 2$V_{meas.}$ = 62(2)°, 2$V_{cal.}$ = 69°. It is insoluble in water, but slowly dissolves in hydrochloric acid. An electron-microprobe analysis yielded an empirical formula, based on 8 O *apfu* and Σ(Mg + Zn) = 1 *apfu*, of (Mg$_{0.95}$Zn$_{0.05}$)$_{\Sigma1.00}$(C$_2$H$_3$O$_3$)$_2$·2H$_2$O, which can be simplified as (Mg,Zn)(C$_2$H$_3$O$_3$)$_2$·2H$_2$O.

Stanevansite is monoclinic with space group $P2_1/c$ and unit-cell parameters a = 11.4927(2), b = 5.85470(10), c = 12.4711(2) Å, β = 91.1610(10)°, V = 838.96(2) Å^3, and Z = 4. It is isostructural with several synthetic glycolate compounds having the general chemical formula M^{2+}(C$_2$H$_3$O$_3$)$_2$·2H$_2$O, where M^{2+} = Co^{2+}, Mn, Zn, and Mg. The crystal structure of stanevansite is characterized by the mononuclear complex [Mg(C$_2$H$_3$O$_3$)$_2$(H$_2$O)$_2$], with such complexes being connected to one another by hydrogen bonds to form a three-dimensional supramolecular architecture. In a [Mg(C$_2$H$_3$O$_3$)$_2$(H$_2$O)$_2$] complex, Mg is octahedrally coordinated by two chelating glycolate ligands and two H$_2$O molecules. Stanevansite represents the first hydrous glycolate mineral and is believed to have formed through the interaction of fluids containing glycolic acid (C$_2$H$_4$O$_3$) derived from decaying plant materials or bacterial activities with Mg produced by the alteration of primary and secondary minerals. Its discovery, together with other glycolate minerals documented recently, namely lazaraskeite Cu(C$_2$H$_3$O$_3$)$_2$, jimkrieghite Ca(C$_2$H$_3$O$_3$)$_2$, and lianbinite (NH$_4$)(C$_2$H$_3$O$_3$)(C$_2$H$_4$O$_3$), not only implies that more glycolate minerals may be found in nature, but also suggests that glycolate minerals may serve as a potential reservoir for biologically fixed carbon.

Keywords: stanevansite, organic mineral, glycolate, crystal structure, X-ray diffraction.

INTRODUCTION

Organic minerals constitute Class 10 in the Nickel-Strunz mineralogical classification and include simple and complex salts of different organic acids (such as formic, acetic, citric, mellitic, methanesulfonic, and oxalic acids), as well as numerous crystalline hydrocarbons, some amides, imides, porphyrines, triazolate complexes, and other compounds (*e.g.*, Mills *et al.* 2009, Echigo & Kimata 2010). In the current list of IMA-approved

---
[§] *Corresponding author e-mail address*: hyang@arizona.edu

Fig. 1. A specimen on which the new mineral stanevansite (indicated by orange arrows) was found.

Fig. 2. A microscopic view of colorless bladed or prismatic crystals of stanevansite, associated with blue lazaraskeite.

minerals, those derived from organic acids include two formates, three acetates, one citrate, one mellitate, one methanesulfonate, four glycolates, and 33 oxalates. In this study, we report a new glycolate mineral species, stanevansite, ideally $Mg(C_2H_3O_3)_2 \cdot 2H_2O$, found in the Santa Catalina Mountains just north of Tucson, Arizona, USA. It is named in honor of Dr. Stanley (Stan) H. Evans, Jr. Dr. Evans developed an interest in minerals during high school, which led him to obtain a B.S. degree in mineralogy from the University of Utah in 1967. He was admitted to graduate school in the same year, but was drafted in early 1968. After serving as a Squadron Administrative Officer and aviator for four years, he returned to the University of Utah and obtained his Ph.D. in igneous petrology and mineralogy in 1978. He then began as a researcher at the University of Utah to study the geochronological aspects of minerals, as well as the rapid growth of II-IV semiconductor compounds, particularly CdS. In 1986, Dr. Evans moved to private industry, retiring as a program manager at Raytheon in Tucson, Arizona, in 2010. Since then, he has volunteered in the mineralogy lab at the University of Arizona, making significant contributions to the construction of the RRUFF database (http://rruff. info) and many other research projects, especially in the determination of the optical and chemical properties of minerals. The new mineral and its name have been approved by the Commission on New Minerals, Nomenclature and Classification (CNMNC) of the IMA (IMA 2022-085). Part of the cotype samples have been deposited at the University of Arizona Alfie Norville Gem and Mineral Museum (Catalogue # 22721) and the RRUFF Project (deposition # R220011).

Metal-glycolate solids have been an attractive subject of numerous investigations. They are mainly prepared as intermediates of chemically and structurally controlled oxide particles (Day *et al*. 1996, Ksapabutr *et al*. 2004, Yu *et al*. 2007, Ng *et al*. 2008, Das *et al*. 2009, Pan *et al*. 2015, Takase *et al*. 2017, 2018) or metals (Chakroune *et al*. 2005, Anzlovar *et al*. 2008, Abdallah *et al*. 2015, 2018, Takahashi *et al*. 2016). They have also been investigated as intrinsic functional materials due to their lightness and various physico-chemical properties. For example, their magnetocaloric properties under low T make them valuable in cryogenic magneto-refrigeration applications (Chen *et al*. 2014), and their chelating properties make them valuable by providing enhanced reactivity in certain catalytic reactions, such as those involved in the polycondensation of ethylene glycol with bis-(hydroxyethyl)terephthalate for the production of poly(ethylene terephthalate), an important thermoplastic material (Biros *et al.* 2002). As there are several coordination variations possible with glycolate molecules (such as bridging, chelating, and terminal modes) (Hubert-Pfalzgraf 1998), metal-glycolate compounds may exhibit different lattice dimensionalities (zero-, one-, two-, or three-dimensional) formed by metal polyhedra. Thus, structures based on isolated nanoclusters, chains, layers, or three-dimensional polymers, including three-dimensional lattices containing shape-controlled cages, can be developed and modified and their open structures can be used for gas storage or separation (Abdallah *et al.* 2018).

In nature, glycolic acid ($C_2H_4O_3$) is a common and abundant organic material that can be generated from several biological sources (see Yang *et al*. 2022 for a summary). It is a product of fixed carbon accumulated in the conversion process of carbon compounds in metabolic pathways. In addition, glycolate can be converted from oxalate, or *vice versa*, through redox reactions either biotically or abiotically. In the human body, the conversion between glycolate and oxalate is
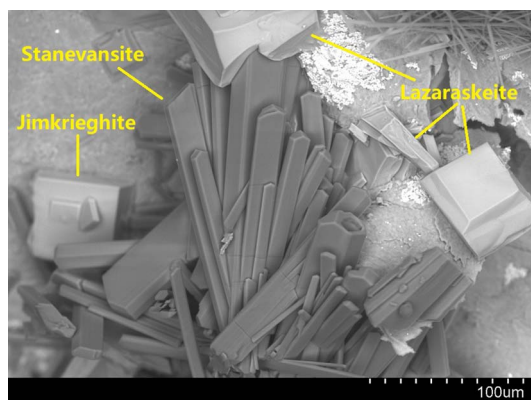
FIG. 3. A backscattered-electron image of bladed or prismatic stanevansite crystals.

intimately associated with obesity and the subsequent development of chronic diseases, including the formation of kidney stones (Knight *et al*. 2010). The conversion between glycolate and oxalate in the metabolic pathways of plants is key to understanding accumulations of biologically fixed carbon (Igamberdiev & Eprintsev 2016). Recently, the abiotic transition between glycolate and oxalate as a redox couple has attracted considerable attention because it demonstrates a carbon-neutral or CO_2-free energy circulation with the help of some metals or oxides as catalysts (Fukushima *et al*. 2018 and references therein). This paper describes the physical and chemical properties, along with the crystal structure, of stanevansite, demonstrating that it is isomorphous with several synthetic hydrous glycolates having general formula $M^{2+}(C_2H_3O_3)_2·2H_2O$ (M = Mg, Zn, Mn, Co) (Fischinger & Webb 1969, Lis 1980, Melikyan *et al*. 2000, Carballo *et al*. 2003, Kennedy *et al*. 2008).

SAMPLE DESCRIPTION AND EXPERIMENTAL METHODS

Occurrence

Stanevansite was found on specimens (Fig. 1) collected at the western end of Pusch Ridge in the Santa Catalina Mountains (32° 21′ 42″ N, 110° 57′ 30″ W, at the elevation of 975 m), north of Tucson, Pima County, Arizona, USA, which is also the type locality for lazaraskeite, $Cu(C_2H_3O_3)_2$ (Yang *et al*. 2022); jimkrieghite, $Ca(C_2H_3O_3)_2$ (Yang *et al*. 2023a); and lianbinite, $(NH_4)(C_2H_3O_3)(C_2H_4O_3)$ (Yang *et al*. 2023b). It occurs in a heavily fractured leucogranite, 1 to 2 m below the rock surface. Associated minerals include lazaraskeite, jimkrieghite, chrysocolla, malachite, wulfenite, mimetite, phosphohedyphane, cerussite, hematite, calcite, microcline, phlogopite, and quartz. Stanevansite is a secondary mineral believed to have formed through the interaction of fluids containing glycolic acid ($C_2H_4O_3$) derived from decaying plant materials or bacterial activities with Mg produced by the alteration of primary and secondary minerals.

Physical and chemical properties and Raman spectra

Stanevansite occurs as sprays of bladed or prismatic crystals elongated along [001], with individual crystals being up to 0.40 × 0.07 × 0.03 mm (Figs. 2 and 3). The common forms are {100}, {010}, {101}, {$\overline{1}$01}. It is colorless in transmitted light and transparent with a white streak and vitreous luster. Stanevansite is brittle and has a Mohs hardness of ~1½; cleavage is perfect on {100}. No parting was observed, but twinning on (100) was detected through single-crystal X-ray analyses. The density, measured by flotation in heavy liquids, is 1.69(5) g/cm^3 and the calculated density is 1.682 g/cm^3 on the basis of the empirical chemical formula and the unit-cell volume determined from single-crystal X-ray diffraction

TABLE 1. ANALYTICAL CHEMICAL DATA (in wt.%) FOR STANEVANSITE

Constituent	Mean	Range	Stand. Dev.	Probe Standard
Mg	10.66	10.42–10.89	0.33	Olivine (Fo92)
Zn	1.45	1.30–1.62	0.17	ZnO
C	22.14			Added in ideal value
O	58.98			Added in ideal value
H	4.64			Added in ideal value
Total	97.87	97.48–98.27	0.48	

Notes: (1) There is insufficient material for the direct measurement of carbon content with the Elemental Combustion System, as we did for lazaraskeite (Yang *et al*. 2022).
(2) The C, H, and O contents were calculated based on the stoichiometry verified by the crystal structure determination.
(3) The six analysis data points were obtained from three different crystals because they were easily damaged by the electron beam, even with the moving stage and large electron beam size.
(4) Trace amounts of Cu and Ca were detected by WDS, but they are below the detection limits (<3σ) of the electron-microprobe analysis.

TABLE 2. X-RAY POWDER DIFFRACTION DATA
(d in Å, I in %) FOR STANEVANSITE

h	k	l	I_{cal}	I_{meas}	d_{cal}	d_{meas}
1	0	0	6.3	7.6	11.461	11.442
2	0	0	6.7	3.8	5.731	5.775
1	0	2	100.0	62.0	5.423	5.47
1	1	0	40.5	92.9	5.211	5.223
1	1	1	73.9	100.0	4.791	4.787
2	0	$\bar{2}$	8.9	15.2	4.261	4.293
1	1	$\bar{2}$	17.1	17.4	4.015	4.008
3	0	0	62.3	73.4	3.820	3.819
0	1	3	7.1	12.5	3.385	3.39
3	0	$\bar{2}$	14.1	7.6	3.287	3.294
1	1	3	6.1	10.3	3.231	3.22
3	1	1	52.2	71.2	3.085	3.102
1	0	$\bar{4}$	45.4	33.2	3.020	3.018
0	2	1	11.7	17.9	2.848	2.845
1	2	0	9.4	19.6	2.835	2.832
0	1	4	5.9	7.1	2.748	2.75
4	0	2	14.0	20.1	2.582	2.58
4	1	1	13.5	9.8	2.511	2.512
2	1	4	7.2	2.7	2.460	2.458
$\bar{2}$	2	2	24.9	33.2	2.412	2.406
1	2	3	3.4	4.9	2.335	2.329
$\bar{3}$	2	1	8.2	6.5	2.289	2.288
1	1	5	5.1	4.4	2.238	2.242
2	2	$\bar{3}$	4.3	4.9	2.216	2.217
5	1	0	7.3	10.3	2.134	2.139
5	1	1	9.2	6.5	2.097	2.101
0	0	6	12.6	15.8	2.075	2.081
4	2	1	15.0	17.9	2.015	2.019
2	0	$\bar{6}$	14.8	17.4	1.964	1.969
1	1	$\bar{6}$	5.2	7.6	1.934	1.927
0	2	5	2.1	1.6	1.896	1.896
0	3	2	2.3	2.7	1.861	1.867
3	2	4	1.6	2.2	1.850	1.853
6	0	2	3.9	3.3	1.816	1.817
4	1	5	3.3	4.4	1.773	1.772
6	1	2	5.0	3.8	1.734	1.734
1	1	7	2.2	3.3	1.678	1.679
4	0	6	3.0	2.2	1.664	1.663
6	1	3	4.4	1.6	1.652	1.645
4	2	$\bar{5}$	5.3	7.6	1.593	1.591
0	0	8	1.4	3.8	1.556	1.554
1	3	5	1.4	3.3	1.519	1.520
$\bar{6}$	1	5	1.1	2.2	1.481	1.478
2	2	7	2.6	2.2	1.463	1.463
3	0	8	1.2	1.1	1.431	1.432
2	4	0	1.0	3.3	1.417	1.417
$\bar{6}$	2	5	1.8	1.6	1.357	1.358
7	2	3	1.7	3.3	1.343	1.343
4	4	0	1.6	2.2	1.303	1.302
$\bar{8}$	2	1	1.0	3.3	1.282	1.282

and the dispersion is very weak with $r > v$. As no k-value (specific molar refractivity) is available for the glycolate group ($C_2H_2O_2$), that derived from the optical data reported for lazaraskeite, $Cu(C_2H_3O_3)_2$ (Yang *et al.* 2022), which is 0.368, was used. This value falls in the range (0.267–0.522) for various organic constituents given by Mandarino (1981). Using this k-value, we obtained the compatibility index for stanevansite, $1 - K_P/K_C = 0.010$ (superior). Stanevansite is insoluble in water, but slowly dissolves in hydrochloric acid at room temperature.

The chemical composition of stanevansite was determined using a CAMECA SX-100 electron microprobe (WDS mode, 15 kV, 10 nA, and 5 µm beam diameter). The standards used for the probe analysis are given in Table 1, along with the measured compositions (n = 6). Stanevansite crystals were easily damaged by the electron beam, even with moving the stage and using a large electron-beam size. The C, H, and O contents were calculated based on the stoichiometry and verified by the crystal structure determination, owing to the fact that there was insufficient material available for the direct measurement of C or H content with an elemental combustion system, as was done for lazaraskeite (Yang *et al.* 2022). The presence of H_2O was also confirmed by Raman spectroscopy (see below). The resultant empirical chemical formula, calculated on the basis of 8 O and $\Sigma(Mg + Zn) = 1$ *apfu* (from the structure determination), is $(Mg_{0.95}Zn_{0.05})_{\Sigma1.00}(C_2H_3O_3)_2 \cdot 2H_2O$, which can be simplified to $(Mg,Zn)(C_2H_3O_3)_2 \cdot 2H_2O$. The ideal formula, $Mg(C_2H_3O_3)_2 \cdot 2H_2O$, requires (wt.%) Mg 11.55, C 22.83, O 60.82, and H 4.80 (total = 100%).

The Raman spectra of two stanevansite were collected from randomly oriented crystals on a Thermo Almega microRaman system using a solid-state laser with a frequency of 532 nm and a thermoelectric cooled CCD detector. The laser is partially polarized with 4 cm^{-1} resolution and a spot size of 1 µm.

X-ray crystallography

Both powder and single-crystal X-ray diffraction data for stanevansite[1] were collected on a Rigaku Xtalab Synergy DS 4-circle diffractometer equipped with Cu$K\alpha$ radiation and operated at 50 kV and 1 mA. Powder X-ray diffraction data were collected in the Gandolfi powder mode at 50 kV and 1 mA (Table 2) and the unit-cell parameters, refined using the program by

data. Optically, stanevansite is biaxial (+), with $\alpha = 1.539(3)$, $\beta = 1.545(5)$, $\gamma = 1.558(5)$, $2V_{meas.} = 65(2)°$, $2V_{cal.} = 69°$. Pleochroism was not observed,

---

[1] Supplementary Data are available from the Depository of Unpublished Data on the MAC website (http://mineralogicalassociation.ca/), document "Stanevansite, CM62, 23-00047".

TABLE 3. COMPARISON OF CRYSTALLOGRAPHIC DATA FOR STANEVANSITE WITH SYNTHETIC ISOSTRUCTURAL COMPOUNDS

	Stanevansite	Synthetic-Mn	Synthetic-Co	Synthetic-Zn
Ideal chemical formula	$Mg(C_2H_3O_3)_2 \cdot 2H_2O$	$Mn(C_2H_3O_3)_2 \cdot 2H_2O$	$Co(C_2H_3O_3)_2 \cdot 2H_2O$	$Zn(C_2H_3O_3)_2 \cdot 2H_2O$
Crystal symmetry	Monoclinic	Monoclinic	Monoclinic	Monoclinic
Space group	$P2_1/c$	$P2_1/c$	$P2_1/c$	$P2_1/c$
a (Å)	11.4927 (2)	11.636 (5)	11.5388 (9)	11.391 (2)
b (Å)	5.85470 (10)	5.918 (2)	5.8330 (4)	5.857 (1)
c (Å)	12.4711 (2)	12.568 (6)	12.4477 (9)	12.511 (2)
β (°)	91.1610 (10)	92.42	91.4537 (14)	91.198 (9)
V (Å³)	838.96 (2)	864.7 (6)	837.53 (11)	834.5 (2)
Z	4	4	4	4
ρ_{cal} (g/cm³)	1.795	1.85	1.943	2.002
2θ range for data collection	≤155.22 (CuKα)	≤60 (MoKα)	≤56.0 (MoKα)	≤57.0 (MoKα)
No. of reflections collected	9218	5514	5031	2102
No. of independent reflections	1775	2528	1964	1751
No. of reflections with $I > 2\sigma(I)$	1590		1602	
No. of parameters refined	159		142	119
R(int)	0.0579	0.0327	0.023	
Final R_1, wR_2 factors [$I > 2\sigma(I)$]	0.035, 0.098	0.041, 0.099	0.024, 0.053	0.030, 0.072
Goodness-of-fit	1.035	1.016	0.94	0.99
Reference	(1)	(2)	(3)	(4)

Note: (1) This study, (2) Melikyan *et al.* (2000), (3) Carballo *et al.* (2003), (4) Kennedy *et al.* (2008).

TABLE 4. FRACTIONAL ATOMIC COORDINATES AND EQUIVALENT ISOTROPIC DISPLACEMENT PARAMETERS ($Å^2$) FOR STANEVANSITE

Atom	x/a	y/b	z/c	U_{iso}*/U_{eq}	Occ. (<1)
Mg	0.76035 (4)	0.13673 (7)	0.65983 (3)	0.0239 (2)	0.962 (3)
Zn	0.76035 (4)	0.13673 (7)	0.65983 (3)	0.0239 (2)	0.038 (3)
C1	0.86674 (16)	−0.2496 (3)	0.53963 (13)	0.0322 (4)	
C2	0.85959 (13)	−0.0454 (3)	0.46590 (12)	0.0275 (3)	
C3	0.50157 (13)	0.2035 (3)	0.62271 (12)	0.0265 (3)	
C4	0.56060 (13)	0.4342 (2)	0.63015 (11)	0.0236 (3)	
O1	0.73021 (11)	0.1015 (2)	0.82262 (10)	0.0356 (3)	
O2	0.91104 (10)	0.2965 (2)	0.69929 (11)	0.0376 (3)	
O3	0.81871 (11)	−0.1958 (2)	0.64098 (9)	0.0348 (3)	
O4	0.80820 (10)	0.13092 (18)	0.49911 (8)	0.0322 (3)	
O5	0.90522 (11)	−0.0636 (2)	0.37644 (9)	0.0398 (3)	
O6	0.58692 (10)	0.02965 (19)	0.63228 (9)	0.0329 (3)	
O7	0.66901 (9)	0.43738 (18)	0.64479 (9)	0.0329 (3)	
O8	0.49786 (9)	0.60824 (17)	0.62242 (9)	0.0292 (3)	
H1A	0.829 (2)	−0.374 (4)	0.5100 (19)	0.049 (6)*	
H1B	0.948 (2)	−0.301 (4)	0.5472 (17)	0.040 (5)*	
H2A	0.4455 (19)	0.195 (4)	0.6803 (17)	0.041 (5)*	
H2B	0.4617 (18)	0.191 (3)	0.5551 (17)	0.034 (5)*	
H3	0.780 (3)	−0.312 (6)	0.660 (3)	0.090 (11)*	
H4	0.553 (2)	−0.111 (4)	0.6299 (17)	0.040 (5)*	
H5	0.976 (3)	0.252 (5)	0.678 (2)	0.066 (8)*	
H6	0.922 (2)	0.369 (4)	0.765 (2)	0.048 (6)*	
H7	0.658 (2)	0.101 (4)	0.841 (2)	0.051 (6)*	
H8	0.764 (2)	0.181 (5)	0.876 (2)	0.062 (7)*	

Holland & Redfern (1997), are $a = 11.4636(4)$, $b = 5.8511(2)$, $c = 12.4526(4)$ Å, $\beta = 91.194(3)°$, and $V = 835.07(4)$ $Å^3$.

Single-crystal X-ray diffraction data for stanevansite were collected from a $0.04 \times 0.02 \times 0.02$ mm fragment. All reflections were indexed on the basis of a monoclinic unit-cell (Table 3). The systematic absences of reflections suggest the unique space group $P2_1/c$. The structure was solved with SHELXT (Sheldrick 2015a) and refined

using SHELX2019 (2015b). All H atoms were located through the difference-Fourier syntheses. To facilitate a direct comparison with isostructural compounds (see below), the labeling of atomic sites and their coordinates were taken from those reported by Kennedy et al. (2008) for synthetic glycolate $Zn^{2+}(C_2H_3O_3)_2 \cdot 2H_2O$.

All non-H atoms were refined anisotropically, with all H atoms refined isotropically. The occupancies of Mg and Zn at the Mg site were refined, yielding a Mg:

TABLE 5. ATOMIC DISPLACEMENT PARAMETERS ($Å^2$) OF STANEVANSITE

Atom	U^{11}	U^{22}	U^{33}	U^{12}	U^{13}	U^{23}
Mg	0.0255 (3)	0.0192 (3)	0.0274 (3)	0.00159 (16)	0.00684 (18)	−0.00133 (16)
Zn	0.0255 (3)	0.0192 (3)	0.0274 (3)	0.00159 (16)	0.00684 (18)	−0.00133 (16)
C1	0.0399 (9)	0.0237 (7)	0.0334 (8)	0.0025 (6)	0.0119 (6)	−0.0026 (6)
C2	0.0259 (7)	0.0295 (8)	0.0274 (7)	0.0002 (6)	0.0055 (5)	0.0001 (6)
C3	0.0300 (8)	0.0230 (7)	0.0265 (7)	−0.0011 (6)	0.0024 (6)	0.0011 (5)
C4	0.0291 (7)	0.0206 (7)	0.0214 (6)	0.0002 (5)	0.0070 (5)	0.0009 (5)
O1	0.0314 (6)	0.0445 (7)	0.0313 (6)	−0.0061 (5)	0.0072 (5)	−0.0035 (5)
O2	0.0275 (6)	0.0413 (7)	0.0444 (7)	−0.0015 (5)	0.0066 (5)	−0.0129 (5)
O3	0.0502 (7)	0.0224 (5)	0.0326 (6)	0.0026 (5)	0.0163 (5)	0.0017 (4)
O4	0.0391 (6)	0.0289 (6)	0.0290 (6)	0.0082 (4)	0.0078 (4)	0.0032 (4)
O5	0.0450 (7)	0.0440 (7)	0.0310 (6)	0.0099 (5)	0.0150 (5)	0.0035 (5)
O6	0.0320 (6)	0.0197 (5)	0.0471 (7)	−0.0020 (4)	0.0020 (5)	−0.0028 (4)
O7	0.0270 (6)	0.0214 (5)	0.0506 (7)	0.0006 (4)	0.0068 (5)	−0.0003 (5)
O8	0.0303 (6)	0.0221 (5)	0.0355 (6)	0.0029 (4)	0.0059 (4)	0.0011 (4)

TABLE 6. SELECTED BOND DISTANCES (Å) IN STANEVANSITE AND SYNTHETIC Zn-ANALOGUE

Stanevansite		Synthetic Zn-analogue*	
Mg–O2	2.0204 (13)	Zn–O2	2.0325 (19)
–O7	2.0561 (11)	–O7	2.0561 (11)
–O3	2.0741 (12)	–O1	2.0974 (18)
–O1	2.0767 (12)	–O3	2.0935 (17)
–O4	2.0894 (11)	–O4	2.1019 (17)
–O6	2.1110 (12)	–O6	2.1531 (19)
<Mg–O>	2.0713	<Zn–O>	2.0902
C2–O5	1.2469 (18)		1.247 (3)
–O4	1.2634 (18)		1.259 (3)
C1–C2	1.509 (2)		1.513 (3)
C1–O3	1.4247 (18)		1.429 (3)
–H1A	0.92 (2)		0.97
–H1B	0.98 (2)		0.97
C3–O8	1.2510 (18)		1.250 (3)
–O7	1.2556 (18)		1.261 (3)
C3–C4	1.514 (2)		1.518 (3)
C3–O6	1.4167 (19)		1.412 (3)
–H2A	0.98 (2)		0.97
–H2B	0.95 (2)		0.97

* Note: The data for the synthetic Zn-analogue of stanevansite were from Kennedy *et al.* (2008).

Zn = 0.96:0.04, consistent with the composition determined from the electron-microprobe analysis. The final refinement statistics are listed in Table 3. Atomic coordinates and displacement parameters are given in Tables 4 and 5, respectively. Selected bond distances are presented in Table 6 and hydrogen bonding geometries in Table 7.

DISCUSSION

Crystal structures

Stanevansite is isostructural with synthetic bis(glycolato)manganese(II) dihydrate, $Mn^{2+}(C_2H_3O_3)_2 \cdot 2H_2O$ (Lis 1980, Melikyan *et al.* 2000); bis(glycolato)cobalt(II) dihydrate, $Co^{2+}(C_2H_3O_3)_2 \cdot 2H_2O$ (Carballo *et al.* 2003); and bis(glycolato)zinc(II) dihydrate, $Zn^{2+}(C_2H_3O_3)_2 \cdot 2H_2O$ (Fischinger & Webb 1969, Kennedy *et al.* 2008) (Table 3). Its crystal structure is characterized by the mononuclear complex $[Mg(C_2H_3O_3)_2(H_2O)_2]$ (Fig. 4a), these being connected to one another by hydrogen bonds to form a three-dimensional supramolecular architecture (Fig. 5). Figure 4a illustrates the configuration of a $[Mg(C_2H_3O_3)_2(H_2O)_2]$ complex in stanevansite, wherein Mg is octahedrally coordinated by two chelating glycolate ligands and two H_2O molecules. For comparison, Figure 4b shows the configuration of the $[Cu(C_2H_3O_3)_2]$ complex in lazaraskeite (Yang *et al.* 2022). Unlike stanevansite, the $[Cu(C_2H_3O_3)_2]$ complexes in lazaraskeite are linked to one another by sharing glycolate $(C_2H_3O_3)^-$ anionic groups to form layers parallel to (101) (Fig. 6), these being joined together by strong hydrogen bonds with O···O distances between 2.67 and 2.83 Å.

Raman spectra

The Raman spectrum for stanevansite is shown in Figure 7. The tentative assignments of major Raman bands for stanevansite were made (Table 8) based on the spectroscopic studies of compounds containing the glycolate ion group $(C_2H_3O_3)^-$ (*e.g.*, Medina *et al.* 2001, Silva *et al.* 2013, Do Nascimento *et al.* 2017, Yang *et al.* 2022). Specifically, the bands between 2760 and 3500 cm^{-1} are attributed to O–H and C–H stretching vibrations in the H_2O and $C_2H_3O_3^-$ glycolic groups and those from 2230 to 2650 cm^{-1} to the O–H···O interactions. A weak band centered at 1619 cm^{-1} stems from the H–O–H bending vibrations within the H_2O molecules. The bands between 1200 and 1540 cm^{-1} are ascribable to the C–O and C–C stretching vibrations in the $C_2H_3O_3^-$ glycolic groups, whereas those between 840 and 1100 cm^{-1} are due to C–OH stretching vibrations, as well as the O–C–O bending vibrations in $C_2H_3O_3^-$ glycolic groups. The bands over the range of 400 to 800 cm^{-1} can be assigned to the Mg–O stretching vibrations, H–C–H

TABLE 7. HYDROGEN-BOND GEOMETRY (Å, °) IN STANEVANSITE

D–H···*A*	*D*–H	H···*A*	*D*···*A*	*D*–H···*A*
C3–H2A···O8[i]	0.98 (2)	2.58 (2)	3.2270 (17)	123.7 (16)
C3–H2B···O8[ii]	0.95 (2)	2.56 (2)	3.2498 (18)	129.5 (15)
O3–H3···O7[iii]	0.85 (4)	1.95 (4)	2.7528 (17)	157 (3)
O6–H4···O8[iii]	0.91 (2)	1.77 (2)	2.6730 (16)	176 (2)
O2–H5···O5[iv]	0.84 (3)	1.89 (3)	2.7003 (17)	161 (3)
O2–H6···O5[v]	0.92 (3)	1.82 (3)	2.7086 (17)	162 (2)
O1–H7···O8[i]	0.86 (3)	1.86 (3)	2.7230 (17)	178 (2)
O1–H8···O4[v]	0.90 (3)	1.95 (3)	2.8323 (17)	169 (3)

Symmetry codes: (i) $-x+1$, $y-1/2$, $-z+3/2$; (ii) $-x+1$, $-y+1$, $-z+1$; (iii) x, $y-1$, z; (iv) $-x+2$, $-y$, $-z+1$; (v) x, $-y+1/2$, $z+1/2$.
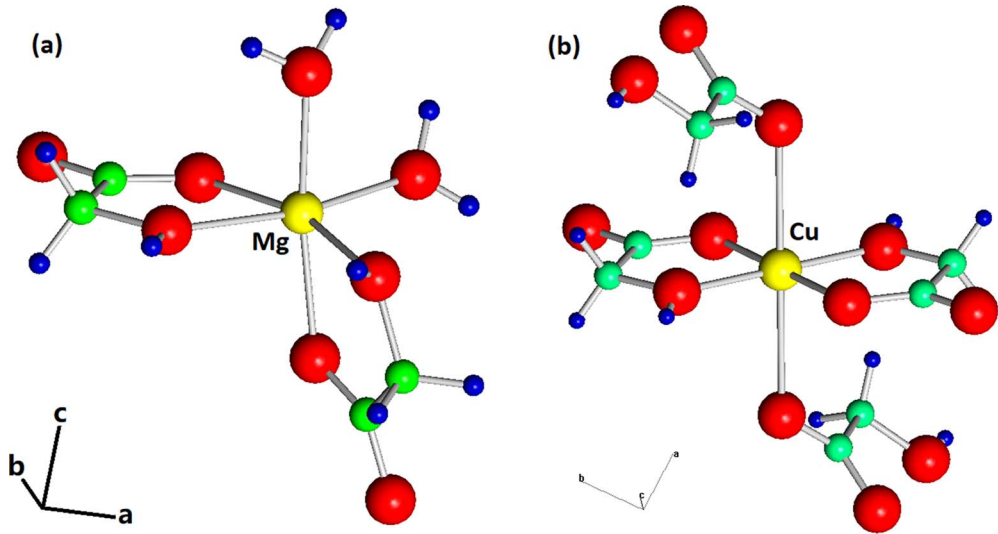
FIG. 4. The configurations of (a) Mg and (b) Cu in octahedral coordination in stanevansite and lazaraskeite (Yang *et al*. 2022), respectively. The red, green, and blue spheres represent O, C, and H atoms, respectively.
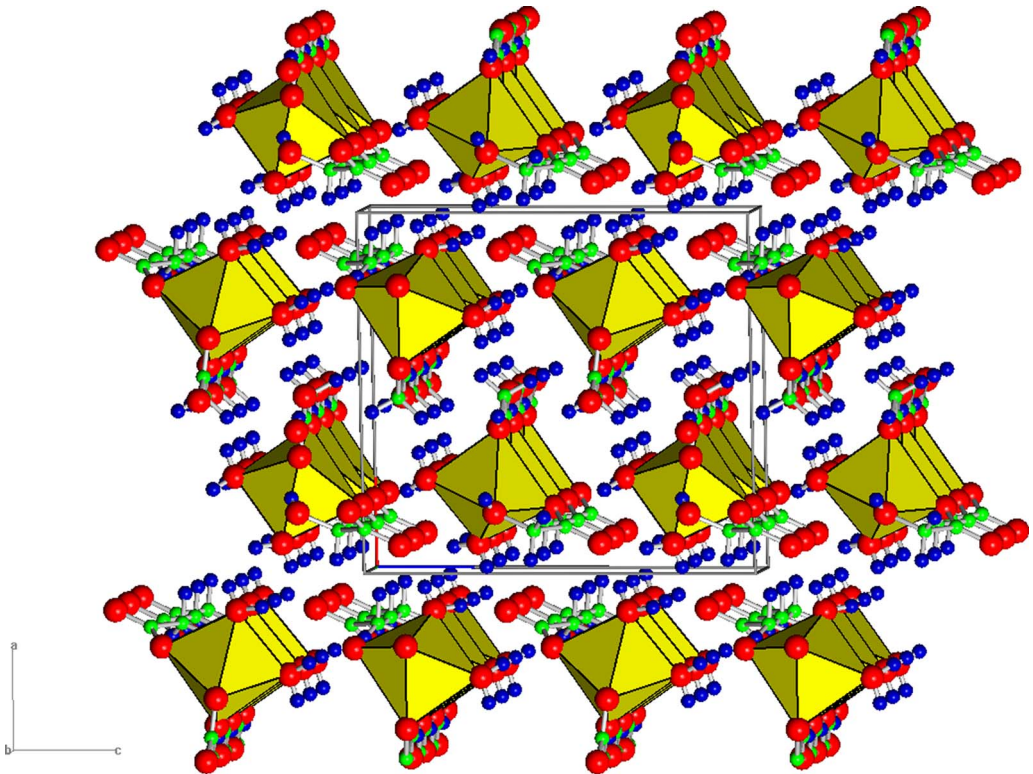
FIG. 5. The crystal structure of stanevansite. Mononuclear complexes of the type [Mg(C$_2$H$_3$O$_3$)$_2$(H$_2$O)$_2$] are connected to one another by hydrogen bonds (not shown for clarity) to form a three-dimensional supramolecular architecture. Yellow octahedra and red, green, and blue spheres represent MgO$_6$, O, C, and H atoms, respectively.
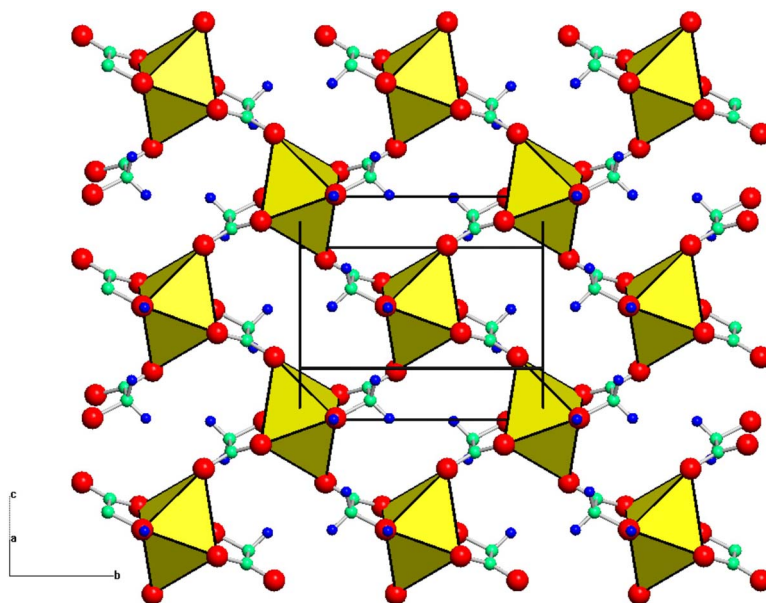
FIG. 6. The [Cu(C$_2$H$_3$O$_3$)$_2$] complexes in lazaraskeite-M_1 are linked to one another by sharing glycolate (C$_2$H$_3$O$_3$)$^-$ anionic groups to form layers parallel to (101). Yellow octahedra and *in situ* red, green, and blue spheres represent CuO$_6$, O, C, and H atoms, respectively.

bending vibrations, and C–C–O bending vibrations in C$_2$H$_3$O$_3$$^-$ glycolic groups. The bands below 400 cm^{-1} are mainly associated with the rotational and translational modes of H$_2$O and C$_2$H$_3$O$_3$$^-$ glycolic groups, as well as the Mg–O interactions and lattice vibrational modes. For comparison, the Raman spectrum of lazaraskeite-M_1 (http://rruff.info/R180026) from the RRUFF Project is also given in Figure 7.

Silva *et al.* (2013) synthesized a hydrous Mg-glycolate with 2.2H$_2$O *pfu* [Mg(C$_2$H$_3$O$_3$)$_2$·2.2H$_2$O]. Although no unit-cell parameters or crystal symmetry were given for this compound, its powder X-ray diffraction pattern is noticeably different from that for stanevansite, as illustrated in Figure 8. As the two materials only differ by 0.2H$_2$O *pfu* in chemistry, the possibility that Mg(C$_2$H$_3$O$_3$)$_2$·2H$_2$O may exist in at least two polymorphs cannot be ruled out.

Stanevansite is isotypic with several synthetic glycolates, including Mn^{2+}(C$_2$H$_3$O$_3$)$_2$·2H$_2$O (Lis 1980, Melikyan *et al.* 2000), Co^{2+}(C$_2$H$_3$O$_3$)$_2$·2H$_2$O (Carballo *et al.* 2003), and Zn^{2+}(C$_2$H$_3$O$_3$)$_2$·2H$_2$O (Fischinger & Webb 1969, Kennedy *et al.* 2008) (Table 3),
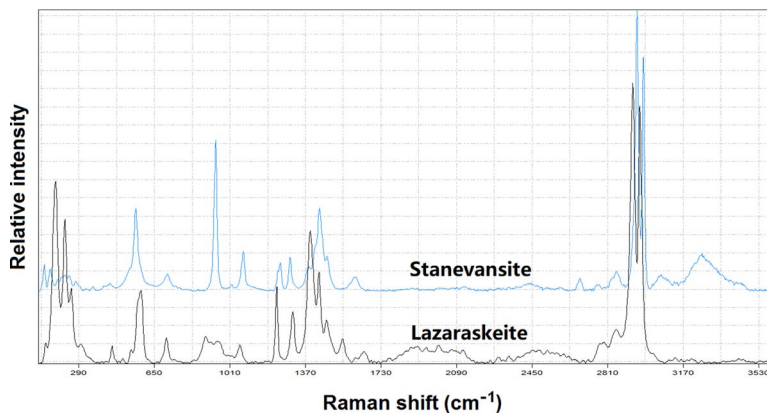
FIG. 7. The Raman spectra of stanevansite and lazaraskeite.

TABLE 8. TENTATIVE ASSIGNMENTS OF MAJOR RAMAN BANDS FOR
STANEVANSITE

Bands (cm^{-1})	Assignment
2760–3500	C–H and O–H stretching vibrations
2230–2650	O–H···O interaction
1619	H–O–H bending vibrations within H_2O
1200–1540	C–O and C–C stretching vibrations in the $C_2H_3O_3^-$ glycolic group
840–1100	C–OH stretching vibrations, as well as and O–C–O bending vibrations in $C_2H_3O_3^-$ glycolic group
400–800	Mg–O stretching vibrations, H–C–H bending vibrations, and C–C–O bending vibrations in $C_2H_3O_3^-$ glycolic group
<400	Lattice and O–Mg–O bending vibrational modes

pointing to the likelihood that a wide range of solid solutions (Mg-Zn-Mn-Co) may exist among these compounds. In fact, stanevansite examined in this study shows a substitution of ∼5% Zn (*apfu*) for Mg. Hence, the discovery of stanevansite lends further support to the implication proposed by Yang *et al.* (2022) that glycolate minerals may be rather widespread and serve as a potential reservoir for biologically fixed carbon in nature. As glycolate is more stable in the reduced environments than is oxalate, the latter usually contributing to the formation of various minerals on the ground surface or in close proximity to decaying

plants, one would expect more glycolate minerals to develop near the subsurface.

As for the geological processes for the formation of stanevansite and other glycolate minerals, the most likely scenario may be as follows: Underground water or fluids containing glycolic acid ($C_2H_4O_3$) derived from C3-type plants [this being based on $\delta^{13}C$ ‰ values that range from -35.1 to -37.7, as measured in lazaraskeite (Yang *et al.* 2022)] flowed along cracks or fractures in rocks. Depending on where they passed, the fluids would incorporate and carry other elements with them. Given the relatively dry and hot weather in Arizona, as well as the
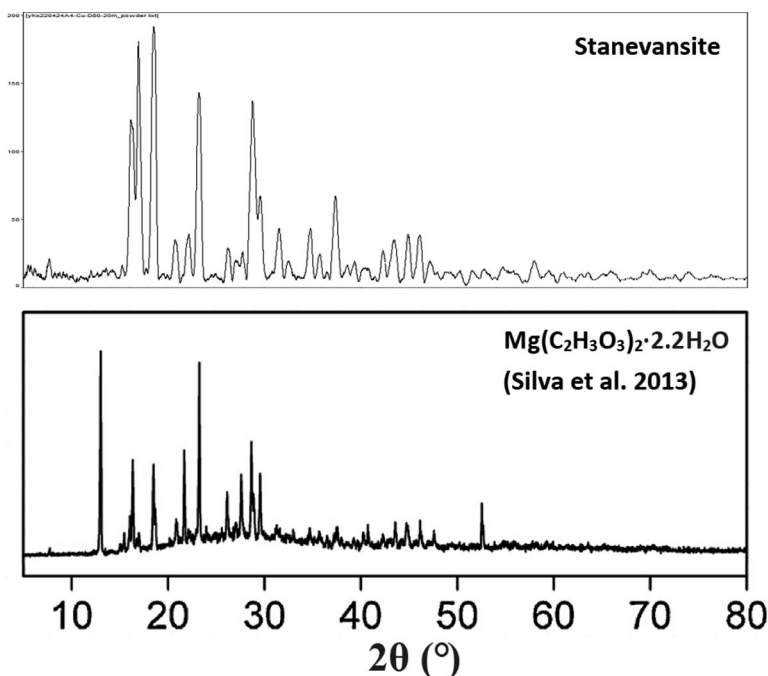
FIG. 8. Comparison of powder X-ray diffraction patterns between stanevansite and synthetic $Mg(C_2H_3O_3)_2 \cdot 2.2H_2O$ (Silva *et al.* 2013).

associated high elevation, such fluids would be expected to evaporate quickly, resulting in the precipitation of various glycolate minerals. In other words, a relatively fast evaporation process of fluids containing glycolic acid ($C_2H_4O_3$) seems to be essential to keep glycolate from being oxidized to oxalate. Nevertheless, it is uncertain whether it is the dry and hot weather, or the high elevation, or the combination of the two factors that is responsible for the formation of glycolate minerals. Regardless, the fact that stanevansite and other glycolate minerals have only been discovered to date in the desert at a relatively high elevation points to a rather special and unique geological environment for the formation of glycolate minerals.

ACKNOWLEDGMENTS

REFERENCES

ABDALLAH, A., AMMAR, S., BAN, V., SIBILLE, R., & FRANCOIS, M. (2018) *Ab initio* structure determination of [Eu$_5$(C$_2$H$_4$O$_2$)$_6$(CH$_3$CO$_2$)$_3$]$_n$ by X-ray powder diffraction. *Acta Crystallographica* **B74**, 592–597.

ABDALLAH, A., GAUDISSON, T., SIBILLE, R., NOWAK, S., CHEIKHROUHOU-KOUBAA, W., SHINODA, K., FRANCOIS, M., & AMMAR, S. (2015) Structural and magnetic properties of mixed Co-Ln (Ln = Nd, Sm, Eu, Gd and Ho) diethyleneglycolate complexes. *Dalton Transactions* **44**, 16013–16023.

ANZLOVAR, A., OREL, Z.C., & ZIGON, M. (2008) Morphology and particle size of di(ethylene glycol) mediated metallic copper nanoparticles. *Journal of Nanoscience and Nanotechnology* **8**, 3516–3525.

BIROS, S.M., BRIDGEWATER, B.M., VILLEGES-ESTRADA, A., TANSKI, J.M., & PARKIN, G. (2002) Antimony ethylene glycolate and catecholate compounds: Structural characterization of polyesterification catalysts. *Inorganic Chemistry* **41**, 4051–4057.

CARBALLO, R., CASTINEIRAS, A., COVELO, B., GARCIA-MARTINEZ, E., & VAZQUEZ-LOPEZ, E.M. (2003) (OC-6-32)-Diaquabis(glycolato)cobalt(II). *Acta Crystallographica* **E59**(8), 588–590. DOI: https://doi.org/10.1107/S1600536803015083

CHAKROUNE, N., VIAU, G., AMMAR, S., JOUINI, N., GREDIN, P., VAULAY, M.J., & FIEVET, F. (2005) Synthesis, characterization and magnetic properties of disk-shaped particles of a cobalt alkoxide: Co-II(C$_2$H$_4$O$_2$). *New Journal of Chemistry* **29**, 355–361.

CHEN, Y.C., GUO, F.S., LIU, J.L., LENG, J.D., VRABEL, P., ORENDAC, M., PROKLESKA, J., SECHOVSKY, V., & TONG, M. L. (2014) Switching of the magnetocaloric effect of Mn-II glycolate by water molecules. *Chemistry-A European Journal* **20**, 3029–3035.

DAS, J., EVANS, I.R., & KHUSHALANI, D. (2009) Zinc glycolate: A precursor to ZnO. *Inorganic Chemistry* **48**, 3508–3510.

DAY, V.W., EBERSPACHER, T.A., FREY, M.H., KLEMPERER, W.G., LIANG, S., & PAYNE, D.A. (1996) Barium titanium glycolate: A new barium titanate powder precursor. *Chemistry of Materials* **8**, 330–332.

DO NASCIMENTO, A.L.C.S., TEIXEIRA, J.A., NUNES, W.D.G., GOMES, D.J.C., GAGLIERI, C., TREU-FILHO, O., PIVATTO, M., CAIRES, F.J., & IONASHIRO, M. (2017) Thermal behavior of glycolic acid, sodium glycolate and its compounds with some bivalent transition metal ions in the solid state. *Journal of Thermal Analysis and Calorimetry* **130**, 1463–1472.

ECHIGO, T. & KIMATA, M. (2010) Crystal chemistry and genesis of organic minerals: A review of oxalate and polycyclic aromatic hydrocarbon minerals. *The Canadian Mineralogist* **48**, 1329–1358.

FISCHINGER, A.J. & WEBB, L.E. (1969) Crystal Structure of diaquobisglycollatozinc(II). *Chemical Communications* **8**, 407–408.

FUKUSHIMA, T., KITANO, S., HATA, S., & YAMAUCHI, M. (2018) Carbon-neutral energy cycles using alcohols. *Science and Technology of Advanced Materials* **19**, 142–152.

HOLLAND, T.J.B. & REDFERN, S.A.T. (1997) Unit cell refinement from powder diffraction data: The use of regression diagnostics. *Mineralogical Magazine* **61**, 65–77.

HUBERT-PFALZGRAF, L.G. (1998) Some aspects of homo and heterometallic alkoxides based on functional alcohols. *Coordination Chemistry Reviews* **178**, 967–997.

IGAMBERDIEV, A.U. & EPRINTSEV, A.T. (2016) Organic acids: The pools of fixed carbon involved in redox regulation and energy balance in higher plants. *Frontiers in Plant Science* **7**, 1–15.

KENNEDY, P., FRANCIS, N., ROVNYAK, D., & KASTNER, M.E. (2008) Redetermination of cis-diaqua-diglycolatozinc(II). *Acta Crystallographica* **E64**(Pt 12), m1635. DOI: https://doi.org/10.1107/S1600536808039585

KNIGHT, J., ASSIMOS, D.G., EASTER, L., & HOLMES, R.P. (2010) Metabolism of fructose to oxalate and glycolate. *Hormone and Metabolic Research* **42**, 868–873.

KSAPABUTR, B., GULARI, E., & WONGKASEMJIT, S. (2004) One-pot synthesis and characterization of novel sodium tris (glycozirconate) and cerium glycolate precursors and their pyrolysis. *Materials Chemistry and Physics* **83**, 34–42.

LIS, T. (1980) Structure of manganese(II) glycolate dihydrate. *Acta Crystallographica* **B36**, 701–703. DOI: https://doi.rog/10.1107/S0567740880004190

MANDARINO, J.A. (1981) The Gladstone-Dale relationship. IV. The compatibility concept and its application. *The Canadian Mineralogist* **19**, 441–450.

MEDINA, G., BERNÈS, S., MARTÍNEZ, A., & GASQUE, L. (2001) Infrared assignment of bis(glycolato)-bis(pyridine) metal(ii) compounds and crystal structure of *trans*bis(glycolato)-*cis*-bis(pyridine)nickel(ii) dihydrate. *Journal of Coordination Chemistry* **54**, 267–284.

MELIKYAN, G.G., AMIRYAN, F., VISI, M., HARDCASTLE, K.I., BALES, B.L., ASLANYAN, G., & BADANYAN, S.H. (2000) Manganese(II):(III) glycolates: Preparation, X-ray crystallographic study, and application in radical cycloaddition reactions. *Inorganica Chimica Acta* **308**, 45–50.

MILLS, S.J., HATERT, F., NICKEL, E.H., & FERRARIS, G. (2009) The standardisation of mineral group hierarchies: Application to recent nomenclature proposals. *European Journal of Mineralogy* **21**, 1073–1080.

NG, S.H., CHEW, S.Y., SANTOS, D.I., CHEN, J., WANG, J.Z., DOU, S.X., & LIU, H.K. (2008) Hexagonal-shaped tin glycolate particles: A preliminary study of their suitability as Li-ion insertion electrodes. *Chemistry-An Asian Journal* **3**, 854–861.

PAN, G.H., HAYAKAWA, T., NOGAMI, M., HAO, Z., ZHANG, X., QU, X., & ZHANG, J.H. (2015) Zinc titanium glycolate acetate hydrate and its transformation to zinc titanate microrods: Synthesis, characterization and photocatalytic properties. *RSC Advances* **5**, 88590–88601.

SHELDRICK, G.M. (2015a) SHELXT – Integrated space-group and crystal structure determination. *Acta Crystallographica* **A71**, 3–8.

SHELDRICK, G.M. (2015b) Crystal structure refinement with SHELX. *Acta Crystallographica* **C71**, 3–8.

SILVA, R.C., CAIRES, F.J., GOMES, D.J.C., GIGANTE, A.C., & IONASHIRO, M. (2013) Synthesis, characterization and thermal studies of alkaline earth glycolate, except beryllium and radium. *Thermochimica Acta* **573**, 170–174.

TAKAHASHI, K., YOKOYAMA, S., MATSUMOTO, T., HUAMAN, J.L.C., KANEKO, H., PIQUEMAL, J.-Y., MIYAMURA, H., & BALACHANDRAN, J. (2016) Towards a designed synthesis of metallic nanoparticles in polyols – Elucidation of the redox scheme in a cobalt-ethylene glycol system. *New Journal of Chemistry* **40**, 8632–8642.

TAKASE, K., NISHIZAWA, H., ONDA, A., YANAGISAWA, K., & YIN, S. (2017) Synthesis and characterization of glycolate precursors to $MTiO_3$ (M = Ni^{2+}, Co^{2+}, Zn^{2+}). *Journal of Asian Ceramic Society* **5**, 482–488.

TAKASE, K., NISHIZAWA, H., IMAMURA, K., ONDA, A., YANAGISAWA, K., & YIN, S. (2018) Synthesis of novel layered zinc glycolate and exchange of ethylene glycol with manganese acetate complex. *Bulletin of the Chemical Society of Japan* **91**, 1546–1552.

YANG, H., GU, X., LAZAR, W., GIBBS, R.B., & DOWNS, R.T. (2023a) Jimkrieghite, IMA2022-138. *CNMNC Newsletter 72, European Journal of Mineralogy* **35**(2), 285–293. DOI: https://doi.org/10.5194/ejm-35-285-2023

YANG, H., GU, X., LAZAR, W., GIBBS, R.B., & DOWNS, R.T. (2023b) Lianbinite, IMA2023-016. *CNMNC Newsletter 73, European Journal of Mineralogy* **35**, 397–402. DOI: https://doi.org/10.5194/ejm-35-397-2023

YANG, H., GU, X., GIBBS, R.B., EVANS, S.H., DOWNS, R.T., & JIBRIN, Z. (2022) Lazaraskeite, $Cu(C_2H_3O_3)_2$, the first organic mineral containing glycolate, from the Santa Catalina Mountains, Tucson, Arizona, U.S.A. *American Mineralogist* **107**, 509–516.

YU, H.K., EUN, T.H., YI, G.R., & YANG, S.M. (2007) Multifaceted titanium glycolate and titania structures from room-temperature polyol process. *Journal of Colloid and Interface Science* **316**, 175–182.